J. Fluid Mech. (1989), *vol.* 205, *pp.* 195–214
Printed in Great Britain

Comparison of a pressure–strain rate theory with simulations

By J. WEINSTOCK

Aeronomy Laboratory, National Oceanic and Atmospheric Administration,
Boulder, CO 80303, USA

(Received 13 April 1988 and in revised form 19 December 1988)

A theoretical expression for the slow part (the nonlinear fluctuation part) of the pressure–strain rate is compared with simulations of anisotropic homogeneous flows. The purpose is to determine the quantitative accuracy of the theory and to test its qualitative predictions that the generalized Rotta coefficient, a non-dimensionalized ratio of slow term to kinetic energy anisotropy, varies with direction and can be negative (this is counter to isotropy return). Comparisons are made between theoretical and simulated values of the slow term and of the generalized Rotta coefficients. Also compared to simulations is an extension of the theory to account for non-stationary turbulence fields. The implication of the comparison for two-point closure theories and for Reynolds stress modelling is pointed out.

1. Background and introduction

The pressure–strain rate tensor ϕ_{ij} is a difficult but key term of the Reynolds stress equation. For an incompressible flow, this term is usually divided into two parts – the so-called slow term (the return to isotropy term) ϕ_{ij}^{s} and the rapid term ϕ_{ij}^{R} (e.g. Lumley 1978; Launder, Reece & Rodi 1975; Reynolds 1976). This article concerns the slow term. Until fairly recently, the slow term was almost universally modelled by the Rotta expression (Rotta 1951)

$$\phi_{ij}^{\mathrm{s}} = -C\epsilon b_{ij} \quad \text{(empirical model)}, \tag{1}$$
$$b_{ij} \equiv \langle u_i u_j \rangle / q^2 - \tfrac{1}{3}\delta_{ij},$$

where ϵ is the dissipation rate of kinetic energy density, b_{ij} is the anisotropy of stress, δ_{ij} is the Kronecker delta, u_i is the velocity fluctuation along Cartesian direction i, $q^2 \equiv \langle u_i u_i \rangle$ is twice the kinetic energy density, and C is an empirical dimensionless constant – the Rotta constant. However, Lumley (1978) has shown that C is not constant. More recently, it was confirmed (Weinstock 1982) that C is not constant, and, additionally, differs for different direction components i and j. Variations with ij were found independently by Cambon, Jaendel & Mathieu (1981). These variations of C occur because ϕ_{ij}^{s} depends on more than one scale of the turbulence and, in addition, the scales generally vary with direction. To account for these scales, ϕ_{ij}^{s} was derived by a two-point closure theory (Weinstock 1981; 1982) – for the case of homogeneous, quasi-stationary turbulence. The principal result of this theory is a relationship between ϕ_{ij}^{s} and an integral over scalar spectra $E(k)$. The purpose of our article is to test the theoretical ϕ_{ij}^{s} by comparison with numerical simulations. Simulations provide a rigorous test of the pressure–strain rate theory, a test which cannot, as yet, be provided by laboratory experiment. The simulation flows

considered are homogeneous shear and strain, and only the normal (diagonal) components $\phi^s_{\alpha\alpha}$ (α is not summed on) are investigated here.

Two curious predictions to be tested are whether $C_{\alpha\alpha}$ can be significantly different for different directions α, and whether $C_{\alpha\alpha}$ can be negative (implying a tendency away from isotropy). Of foremost importance, however, is to investigate the quantitative accuracy of the theoretical $\phi^s_{\alpha\alpha}$ and $C_{\alpha\alpha}$.

To some extent, a test of the theoretical ϕ^s_{ij} is also a test of more elaborate, complete two-point closures such as the DIA (direct interaction approximation, Kraichnan 1959) and the EDQNM (eddy damped-quasi normal, theory, e.g. Orszag 1970; Cambon *et al.* 1981) since these closures all have in common a basic neglect of two-time fourth-order velocity cumulants. The difference is that the more complete closures determine the spectrum $E(k)$ whereas the present closure does not – only the relationship between ϕ^s_{ij} and $E(k)$ is determined. For application of the theory to single-point modelling an appropriate spectrum has previously been given (Weinstock 1981, 1982), and, for the sake of completeness, is discussed in §3 of the present article.

2. Theory and simulation

The theoretical slow-term relation under consideration is given by (Weinstock 1981, 1982; Weinstock & Burk 1985)

$$\phi^s_{ij} = -1.08\left(\frac{2\pi}{3}\right)^{\frac{1}{2}}\frac{1}{q}\int_0^\infty \mathrm{d}k_a \int_0^\infty \mathrm{d}k_b \frac{k_a^2 k_b^2 E(k_b)\,[E_{ij}(k_a) - \frac{1}{3}E(k_a)\,\delta_{ij}]}{(k_a^2+k_b^2)^{\frac{3}{2}}H^{-1}}, \tag{2}$$

$$E(k) \equiv \tfrac{1}{2}[E_{11}(k)+E_{22}(k)+E_{33}(k)],$$

$$H \equiv \left[2 - \frac{2.4k_b^2}{k_a^2+k_b^2} - 0.08\left(\frac{4k_a k_b}{k_a^2+k_b^2}-1\right) + \frac{2}{3}\left(1-\frac{2k_a^2}{k_a^2+k_b^2}\right)\right].$$

Here $E_{ij}(k)$ is the scalar spectrum of the two-point velocity fluctuation tensor; i.e. $E_{ij}(k)$ is the spherical integral over a k-shell of the velocity spectrum $\langle u_i(\boldsymbol{k},t)\,u_j^*(\boldsymbol{k},t)\rangle\, V^{-1}$ where $u_i(\boldsymbol{k},t)$ is the spatial Fourier transform of u_i and V is the volume. The noteworthy feature of this equation is that it shows that ϕ^s_{ij} depends on $E_{ij} - \frac{1}{3}E\delta_{ij}$, the anisotropy of the spectrum, rather than on the anisotropy of kinetic energy. For application of (2) to Reynolds stress modelling, a simpler form of ϕ^s_{ij} was derived (Weinstock 1981, 1982; Weinstock & Burk 1985) by use of a model spectrum.

Equation (2) for ϕ^s_{ij} can be put in the familiar Rotta form

$$\phi^s_{ij} = -C_{ij}\,\epsilon b_{ij} \tag{3}$$

by defining C_{ij} as

$$C_{ij} = 1.08\left(\frac{2\pi}{3}\right)^{\frac{1}{2}}\frac{1}{\epsilon q b_{ij}}\int_0^\infty \mathrm{d}k \int_0^\infty \mathrm{d}k \frac{k_a^2 k_b^2 E(k_b)\,[E_{ij}(k_a) - \frac{1}{3}E(k_a)\,\delta_{ij}]}{(k_a^2+k_b^2)^{\frac{3}{2}}H^{-1}}, \tag{4}$$

where C_{ij} are dimensionless quantities which we refer to as generalized Rotta coefficients.

Our goal is to compare (2) and (4) with numerical simulations of $\rho_0^{-1}\langle p^s(\partial u_i/\partial x_j + \partial u_j/\partial x_i)\rangle \equiv \phi^s_{ij}$ for the normal components $i = j = 1$, 2 or 3. For this comparison, simulation values of spectra are used in (2). What is being tested is whether $\phi^s_{\alpha\alpha}$ is related to $E_{ij}(k)$ in the manner given by (2). Comparisons are made first for a homogeneous shear flow, and, afterwards, for a plane strain, axisymmetric

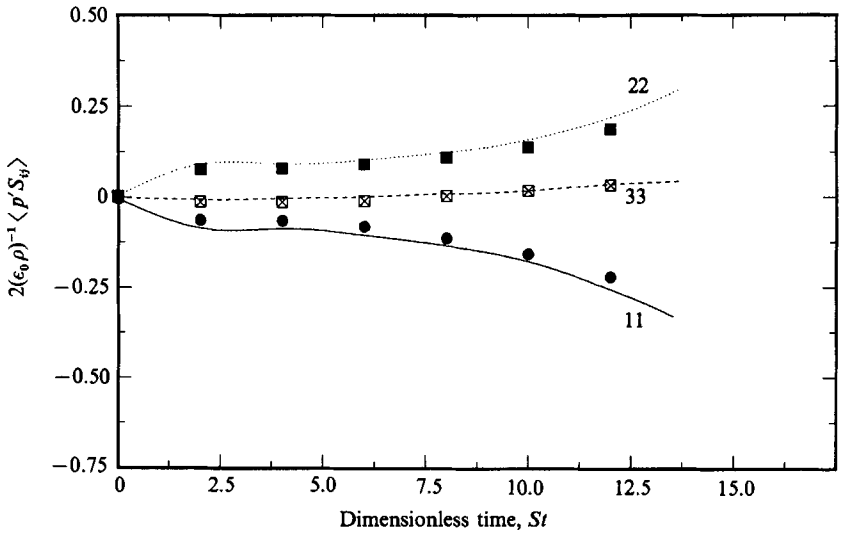

FIGURE 1. $\phi^s_{\alpha\alpha}/\epsilon_0$ versus non-dimensionalized time St for a simulated homogeneous shear flow, showing both simulation (curves) and theory (points): $\alpha = 1$, 2, and 3. S is the mean shear rate $\partial U_1/\partial x_2$.

contraction and axisymmetric expansion. Incidentally, for such flows, J. P. Bertoglio pointed out (private communication, 1987) that, in the original derivation of (2) (Weinstock 1981), the gradients of mean velocity V_0 were not completely accounted for in the time dependence of two-time second moments. This has been corrected and it is found that (2) is not changed in form, but that $E_{\alpha\alpha}(k)$ varies with time. This time variation is determined by the simulation and its influence on $\phi^s_{\alpha\alpha}$ is accounted for in §2.1 and discussed in §3.

2.1. *Comparison for homogeneous shear*

Numerical simulations of homogeneous shear by Rogers, Moin & Reynolds (1986) determine the slow pressure–strain rate term components $\phi^s_{\alpha\alpha} \equiv 2\rho_0^{-1}\langle p^s\,\partial u_\alpha/\partial x_\alpha\rangle$ in a direct fashion. That is, the slow part of the pressure fluctuation, defined by

$$\rho_0^{-1}\nabla^2 p^s = -\nabla\cdot(\boldsymbol{u}\cdot\nabla\boldsymbol{u}), \tag{5}$$

is determined from the simulated $\boldsymbol{u}$. Also determined by the simulations are the spectra $E_{\alpha\alpha}(\boldsymbol{k})$ needed to determine the right-hand side of (2). Hence, simulations supply all the quantities needed to test the theory; i.e. to see if $2\rho_0^{-1}\langle p^s\,\partial u_\alpha/\partial x_\alpha\rangle$ is equal to the right-hand side of (2). Our testing procedure is to calculate the right-hand side of (2) by substituting in the simulation spectra, and then comparing with the value of $\phi^s_{\alpha\alpha} \equiv 2\rho_0^{-1}\langle p^s\,\partial u_\alpha/\partial x_\alpha\rangle$ given directly by the simulations. Respective values of $C_{\alpha\alpha}$ are obtained by dividing $\phi^s_{\alpha\alpha}$ with $(-\epsilon b_{\alpha\alpha})$. Such calculations of (2), or (4), were made for simulation run C128U (Rogers *et al.* 1986), and are displayed in figures 1 and 2. In this run, the turbulence intensities necessarily vary with t, the time elapsed after simulation start-up, and $\phi^s_{\alpha\alpha}$ and $C_{\alpha\alpha}$ were calculated for each of the elapsed time intervals $St = 2, 4, \ldots$, where $S = 28.29$ is the mean shear. Figure 1 contains simulation values of $\phi^s_{\alpha\alpha}$ versus t together with the theoretical values of $\phi^s_{\alpha\alpha}$ obtained from the right-hand side of (2) (We note that p^s is denoted by p' and $(\partial u_i/\partial x_j + \partial u_j/\partial x_i)$ by $2S_{ij}$ in figure 1.) Upon comparison, it is evident in this figure

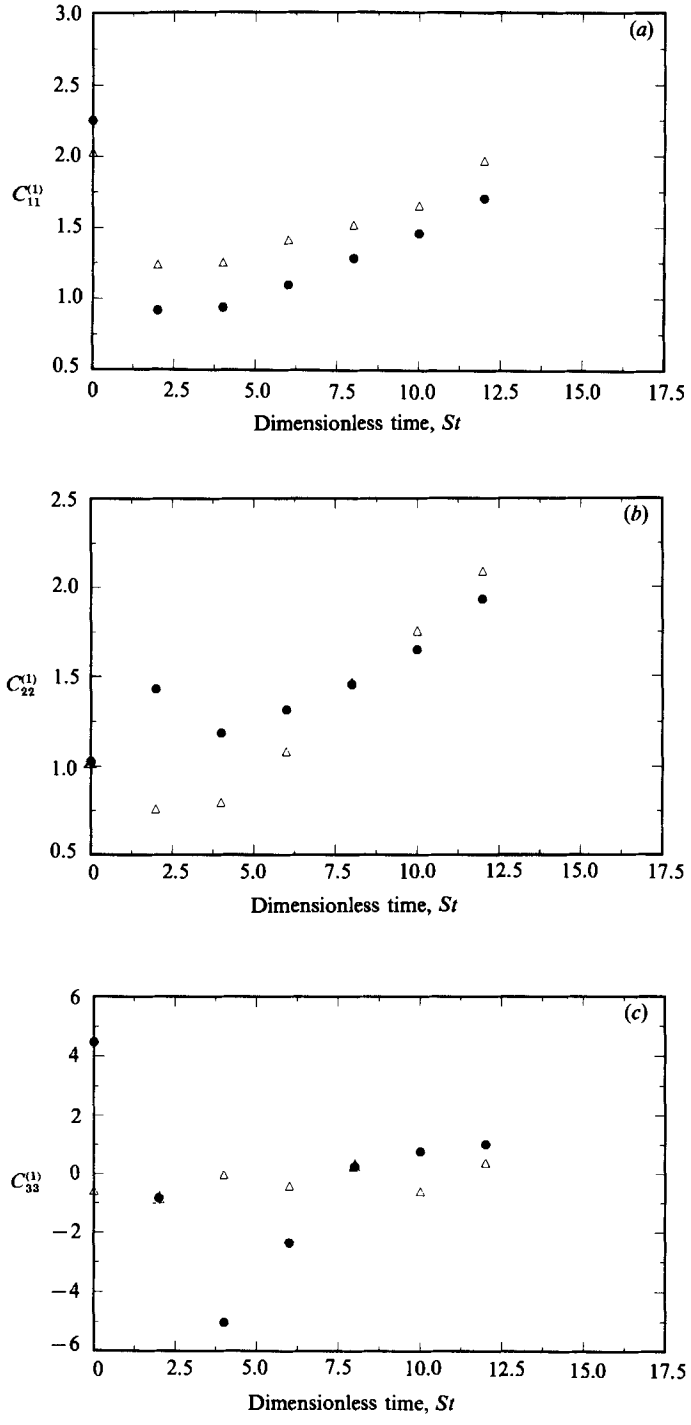

FIGURE 2. $C_{\alpha\alpha}$ versus t for the simulated homogeneous shear flow of figure 1, showing both simulation (▲) and theory (●) values. (*a*), (*b*), (*c*) are for $\alpha = 1, 2, 3$ respectively.

that (2) is close to $\phi^s_{\alpha\alpha} = 2\rho_0^{-1}\langle p^s\,\partial u_\alpha/\partial x_\alpha\rangle$ at all times and for all α. Not shown are the values of $\phi^s_{\alpha\alpha}$ for $St \geqslant 14$ at which time the energy containing scales have grown so large that the simulation size and 'wall effects' have become significant.

Although figure 1 tends to corroborate the theoretical $\phi^s_{\alpha\alpha}$, a more illuminating comparison is for the generalized Rotta coefficients $C_{\alpha\alpha}$ since these have been given much attention in turbulence models, and, more importantly they shed some light on the behaviour of intercomponent energy transfer. The comparison between simulated $C_{\alpha\alpha}$ given by $2\rho_0^{-1}\langle p^s\,\partial u_\alpha/\partial x_\alpha\rangle/(-\epsilon b_{\alpha\alpha})$, and theoretical $C_{\alpha\alpha}$, given by the right-hand side of (4), is made in figures 2(*a*), 2(*b*), and 2(*c*). Noteworthy in these figures are three qualitative features. (i) Each $C_{\alpha\alpha}$ varies substantially within a single flow as the turbulence anisotropy evolves in time (e.g. C_{11} varies from 0.8 to 2.1 as St increases above 4, and C_{33} varies from zero to 0.4 in this same interval). (ii) $C_{\alpha\alpha}$ differs with different direction index α, and the difference can be large (e.g. $C_{33} = 0$, and $C_{11} = 1.5$ at $St = 7$). (iii) $C_{\alpha\alpha}$ can be negative (C_{33} for St between 0 and 6).

The first of these behaviours, i.e. the variation of C_{11} with St, conforms with previous predictions of Lumley (1978). All three behaviours are predicted by present theory. What is unexpected is not the fact that such variations can occur, but, rather, that they all occur, and to so large an extent, in a single and relatively simple flow configuration. These variations occur in both the theory and simulations. Of special note for C_{33}, the simulation values pass through zero more than once and this complicated behaviour is also found in the theoretical values.

As for a quantitative comparison, figures 2(*a*) and 2(*b*) show that the theoretical C_{11} and C_{22} are fairly close to simulated values for almost all points – with the differences less than 0.3. The notable exception is the value of C_{22} at $St = 2$. As for C_{33}, the theoretical values are highly discrepant at the points $St = 0$ and 4, and 6, but are accurate at the points $St = 2$ and 8. However, the inaccurate values, and the accurate values as well, are mitigated by the fact that we had to divide by practically zero in order to obtain C_{33}; i.e. $C_{33} = -\phi^s_{33}/(\epsilon b_{33})$ and $b_{33} \approx 0$. Therefore a small inaccuracy in b_{33} will cause a large error C_{33}, and C_{33} does not provide a quantitative test of the theory. (Incidentally, C_{33} is not a significant parameter of the flow when b_{33} is near zero since, then, ϕ^s_{33}/ϵ is likewise near zero and insensitive to C_{33}. What is remarkable about the predicted C_{33} is that it 'oscillates' about zero going from negative to positive as does the simulation – a very complex behaviour to predict.)

From the perspective of closure theory it is very desirable to see if the discrepant points of C_{22} and C_{33} have a simple cause that can be rectified, e.g. violation of a simple assumption of theory. An obvious cause is that $E_{22}(k)$ changes drastically at early times, varying from a 'top hat' spectrum at $St = 0$ to a broader and more rounded spectrum at $St = 4$ – as shown in figure 3. Such a rapid variation may violate a stationarity condition of the theory. The value of ϕ^s_{33} is particularly sensitive to time variations since b_{33} is a small difference between the two relatively large numbers $\langle u^2\rangle$ and $\frac{1}{3}q^2$.

To investigate the discrepant points, we extend the theory to time-varying E_{ij} and recalculate $C_{\alpha\alpha}$. The extended theory is readily derived in Appendix A to give ϕ^s_{ij} as

$$\phi^s_{ij} = 1.08\left(\frac{2\pi}{3}\right)^{\frac{1}{2}} q^{-1}\int_0^\infty \mathrm{d}k_a \int_0^\infty \mathrm{d}k_b \frac{k_a^2\,k_b^2\sum_r E_{rr}(k_b)}{(k_a^2+k_b^2)^{\frac{3}{2}}H^{-1}}\left[\frac{E_{ij}(k_a)}{1+a_{rj}} - \sum_\alpha \frac{E_{\alpha\alpha}(k_a)\,\delta_{ij}}{3(1+a_{\alpha j})}\right], \tag{6a}$$

$$a_{rj} \equiv \frac{(3\pi/8)^{\frac{1}{2}}}{(k_a^2+k_b^2)^{\frac{1}{2}}}\left[\frac{\partial \ln E_{rr}(k_a)}{\partial t} + \frac{\partial \ln E_{jj}(k_a)}{\partial t}\right] \tag{6b}$$

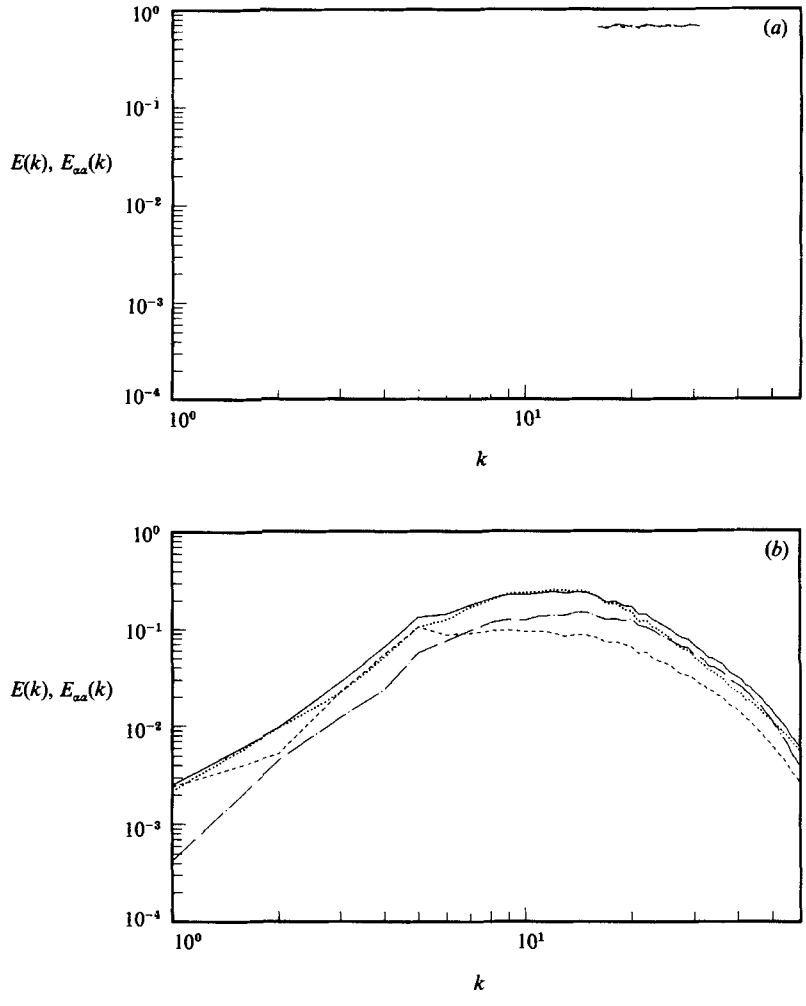

FIGURE 3. Spectra of the simulated flow in figures 1 and 2: (*a*) spectra at $St = 0$; (*b*) at $St = 4$. ——, $E(k)$; · · · · · ·, $E_{11}(k)$; – – – –, $E_{22}(k)$; —·—, $E_{33}(k)$.

(where the sums on r and α run from 1 to 3) provided that the temporal variations are sufficiently slow ($a_{rj}^2 \ll 1$). This equation is the same as (2) except for the time-variation factors a_{ij}, and predicts somewhat different values of $C_{\alpha\alpha}$. To calculate these corrected $C_{\alpha\alpha}$ from (6*a*) we need $\partial \ln E_{\alpha\alpha}/\partial t$, and, since these time derivatives are not readily available, we have used the approximation

$$\frac{\partial \ln E_{\alpha\alpha}}{\partial t} \approx \frac{\partial \ln R_{\alpha\alpha}}{\partial t}. \tag{7}$$

This approximation is crude but, for use in (6), need only be satisfied near the spectral peak of $E_{\alpha\alpha}$ where $E_{\alpha\alpha}$ is proportional to $R_{\alpha\alpha}$. For cases where near peak values of $E_{\alpha\alpha}$ are insufficient for use in (6), an approximation different from (7) is also used – as described in §2.2. This approximation is discussed in Appendix B. The corrected values of $C_{\alpha\alpha}$ are obtained by substitution of (7) in (6*a*). These values are given in figures 4(*a*) and 4(*b*) for the times $St = 2$ and 4 (the initial time $St = 0$ is

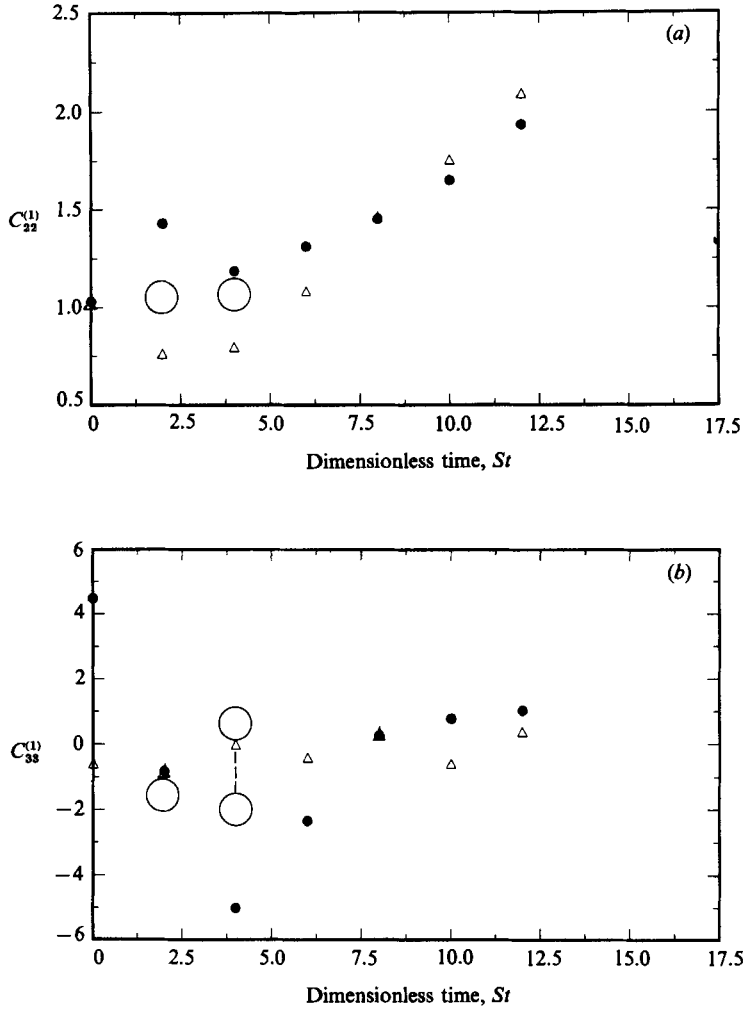

FIGURE 4. Corrected theoretical values of $C_{\alpha\alpha}$ for the simulated homogeneous shear flow: ○, corrected theory: ●, uncorrected theory; △, simulation. (*a*) $\alpha = 2$, (*b*) $\alpha = 3$.

ignored since the $b_{\alpha\alpha}$ and $\phi^{s}_{\alpha\alpha}$ are practically zero and $C_{\alpha\alpha}$ is the inaccurate ratio of two near-zero numbers). It is seen in figure 4 that the two major discrepancies significantly diminish when temporal changes are accounted for. These are C_{22} at $St = 2$ and C_{33} at $St = 4$. The error bar in C_{33} reflects uncertainties of (7) and other approximations. The values of the corrected C_{11} change by less than 10% and are ignored. While we emphasize that the improved values of theoretical C_{22} are only approximate owing to use of (7), these changes do show that correction for non-stationarity is in the right direction and has the proper magnitude to account for the notable discrepancies. The significance of the comparison in figure 4 for closure theory and modelling is discussed in §3.2.

2.2. *Comparison for plane strain*

A comparison of theory with plane-strain simulation is shown in figure 5. The simulation is identified as run PXA (Lee & Reynolds 1985). Figure 5(*a*) shows that

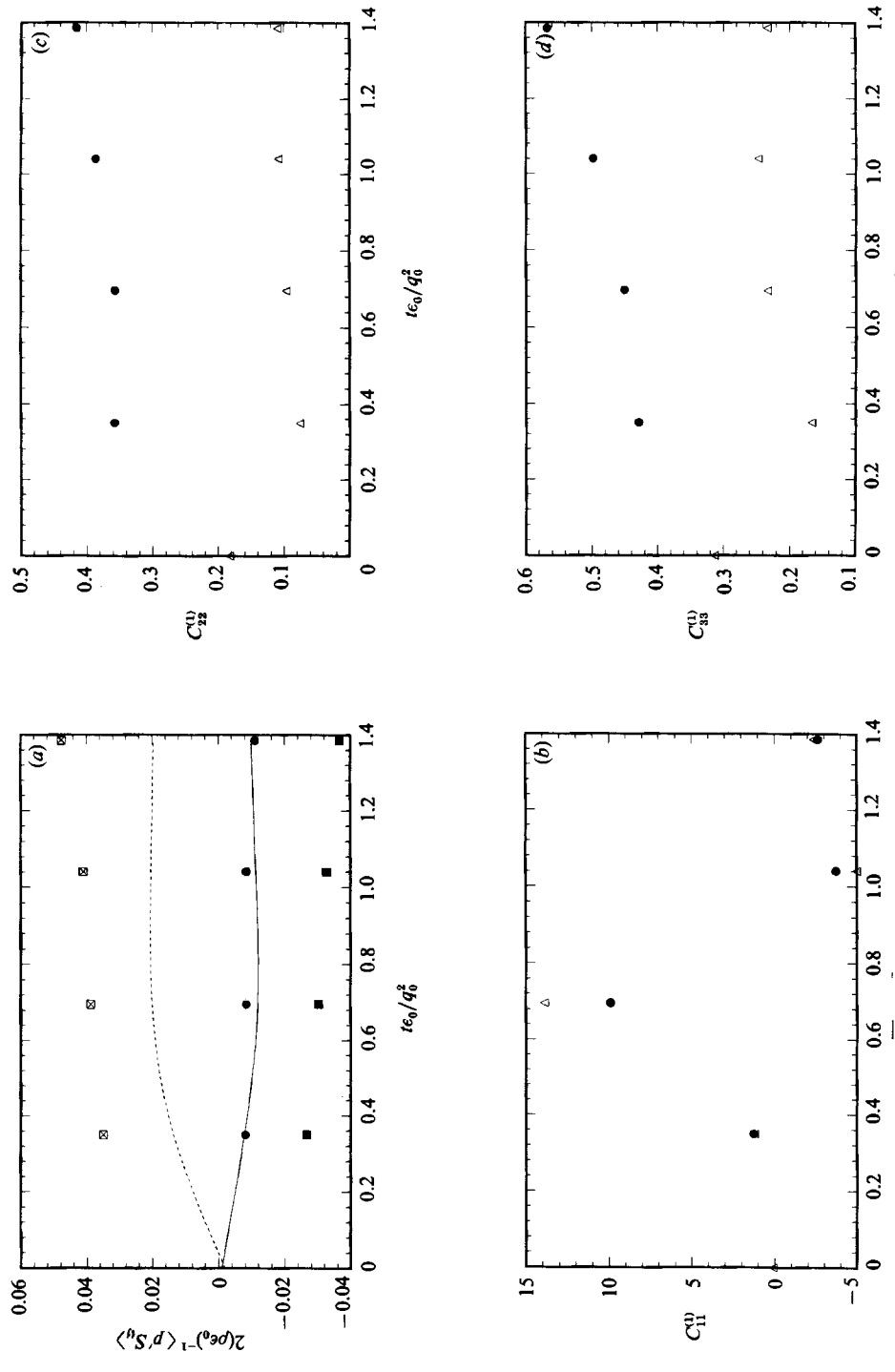

FIGURE 5. $C_{\alpha\alpha}$ and $\phi^s_{\alpha\alpha}/\epsilon_0$ versus non-dimensional $t\epsilon_0/q_0^2$ for a simulated plane strain, showing both theoretical and simulation values. (*a*) ϕ^s_{xx}, theory ●, $\alpha = 1$; ■, 2; ⊠, 3: simulation ——, $\alpha = 1$; ·····, 2; – – –, 3. (*b*), (*c*), (*d*) are for C_{11}, C_{22}, C_{33}, respectively. Here, ϵ_0 and q_0 denote initial values of ϵ and q: ●, theory; △, simulation.

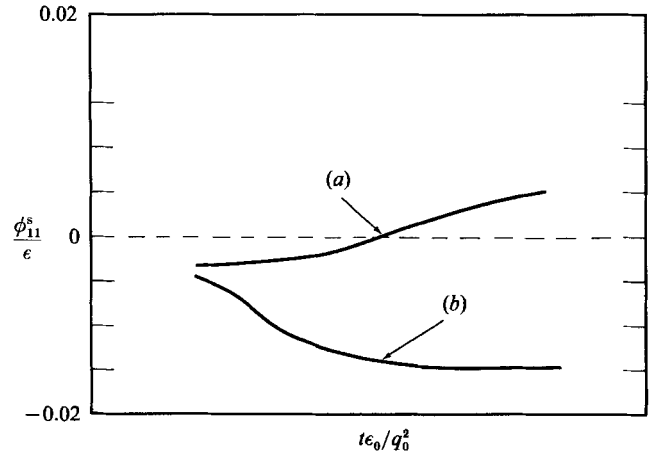

FIGURE 6. ϕ^s_{11}/ϵ_0 versus t for (*a*) the linear Rotta model and (*b*) simulation and theory.

theoretical and simulation $\phi^s_{\alpha\alpha}/\epsilon_0$ are quite close to each other, differing by less than 0.02 for all α and throughout the entire simulation.

As found for homogeneous shear flow, it is seen that $C_{\alpha\alpha}$ generally varies with direction α and can be negative. This is shown in figure 5(*b–d*). What is most remarkable is that the theoretical values of C_{11} follow the complex behaviour of the simulation values, both going from an extremely large positive value to a large-magnitude negative value, passing through zero at virtually the same point. The large magnitudes occur because b_{11} is very close to zero while ϕ^s_{11} remains non-zero. The non-vanishing of ϕ^s_{11} at $b_{11} = 0$ contradicts the linear Rotta model $\phi^s_{11}(\text{Rotta}) = -C\epsilon b_{11}$, which, in figure 5(*b*), would simply have C_{11} be a constant of roughly 1.5 for all t. The Rotta model is contrasted with the actual ϕ^s_{11} in figure 6.

Quantitatively, the ratio of theoretical to simulated values of C_{22} and C_{33} is very large – a factor of 3 in some cases. However, the absolute error (difference) is only about 0.28 which is small compared with typical values used in models, say 1.5. In other words, the relative error is very large but the absolute error is small. We believe that the relative error is irrelevant in this particular case since both theory and simulation magnitudes are both unusually small. Here, it is the absolute value that matters in our opinion. The reader will make his own judgement on this issue. The fact that C_{22} and C_{33} are less than 0.4 is, in itself, unprecedented and a little striking. According to (4), such small values are caused by the low Reynolds number of the simulation, i.e. it was previously shown (Weinstock 1982) that the right-hand side of (4) gives $C_{\alpha\alpha} \propto (1 - R_\nu^{-\frac{1}{2}})$, where $R_\nu \equiv q^3(22\epsilon\nu)^{-1}$ is the Reynolds number and ν is the molecular viscosity. Therefore, $C_{\alpha\alpha}$ decreases markedly as R_ν decreases below about 20.

We would like to know if the discrepancy between theory and simulation could be explained by temporal changes of kinetic energy as determined by (6). The corrected values of C_{22} and C_{33} calculated by (6) are shown in figures 7(*a*) and 7(*b*). As for the case of homogeneous shear, it is seen that the discrepancies significantly diminish when temporal changes are accounted for. Error bars at the point $t\epsilon_0/q_0^2 = 0.35$ reflect the uncertainty in estimated $\partial \ln E_{\alpha\alpha}/\partial t$. This uncertainty, at this time point, is because the spectral shapes are changing very rapidly with time and approximation (7) is inadequate. The lower extrema points at $t\epsilon_0/q_0^2 = 0.35$ in

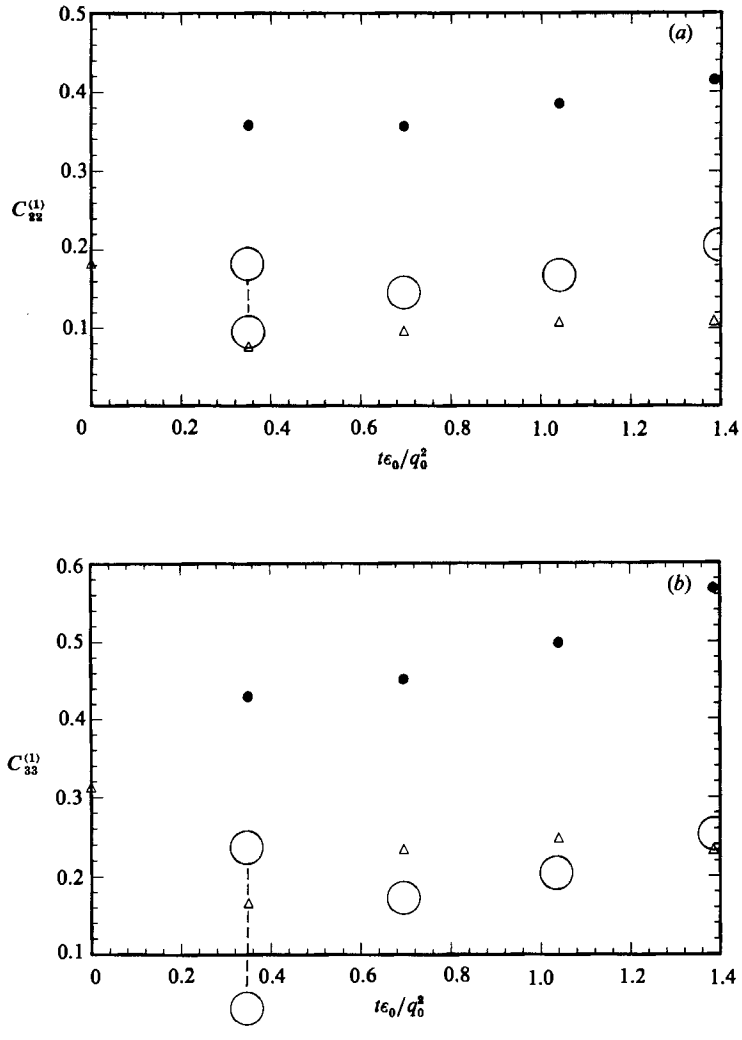

FIGURE 7. Corrected $C_{\alpha\alpha}$ for the plane-strain simulation: ○, corrected theory; ●, uncorrected theory; △, simulation. (*a*) $\alpha = 2$; (*b*) $\alpha = 3$.

figures 7(*a*) and 7(*b*) are for $\partial \ln E_{\alpha\alpha}/\partial t \approx \partial \ln R_{\alpha\alpha}/\partial t$ and the top points are for $\partial \ln E_{\alpha\alpha}/\partial t \approx [E_{\alpha\alpha}(k_a, t+\Delta t) - E_{\alpha\alpha}(k_a, t)]/\Delta t$ where $\Delta t = 0.35q^2/\epsilon_0$, and k_a is taken to be 9, the value near where the integrand of (6) peaks. Although imprecise, the calculated changed in C_{22} and C_{33} show that non-stationarity is sufficiently large to be a possible cause of the discrepancy between theory and simulation. Our reservation about this conclusion is because $\partial E_{\alpha\alpha}/\partial t$ is not known accurately.

2.3. *Axisymmetric contraction*

Calculations of $C_{\alpha\alpha}$ were made for the axisymmetric contraction identified as run AXK by Lee & Reynolds (1985). Theory and simulation values are given in figure 8. As for the plane-strain case, these $C_{\alpha\alpha}$ are all much less than 1.5 because the Reynolds number is low. Theory values exceed simulations by about 0.2 – a comparatively small absolute error (the relative error is large, but of minor significance since $C_{\alpha\alpha}$ is small, as we argued in §2.2). Unlike the plane-strain case, C_{11}

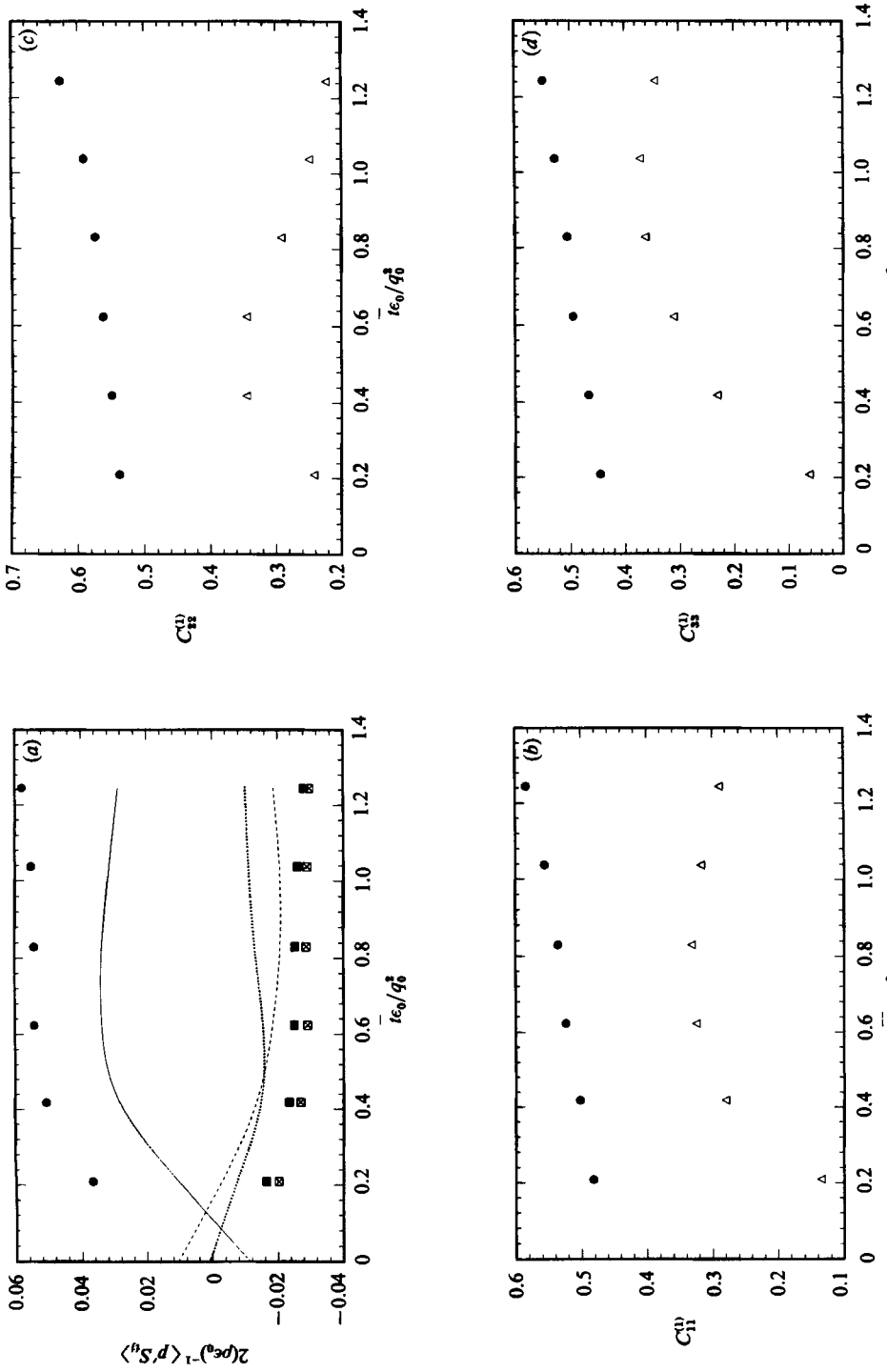

FIGURE 8. C_{xx} and ϕ_{xx}^s/ϵ_0 versus t for a simulated axisymmetric contraction, showing both theory and simulation: (*a*), (*b*), (*c*), (*d*) are for ϕ_{xx}^s, C_{11}, C_{22}, C_{33} respectively. Symbols as in figure 5.

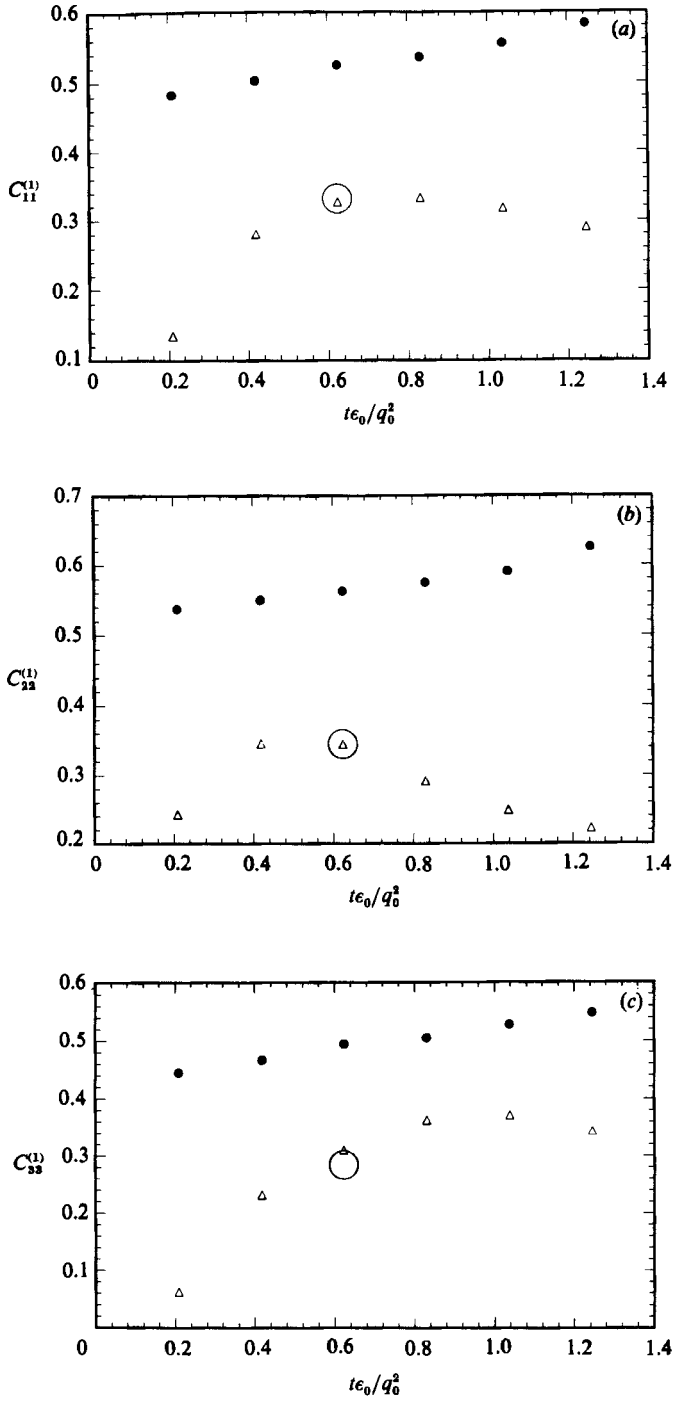

FIGURE 9. Corrected $C_{\alpha\alpha}$ versus t for the axisymmetric contraction: ○, corrected theory at $t\epsilon_0/q_0^2 = 0.62$; ●, uncorrected theory; △, simulation. (*a*) $\alpha = 1$, (*b*) $\alpha = 2$, (*c*) $\alpha = 3$.

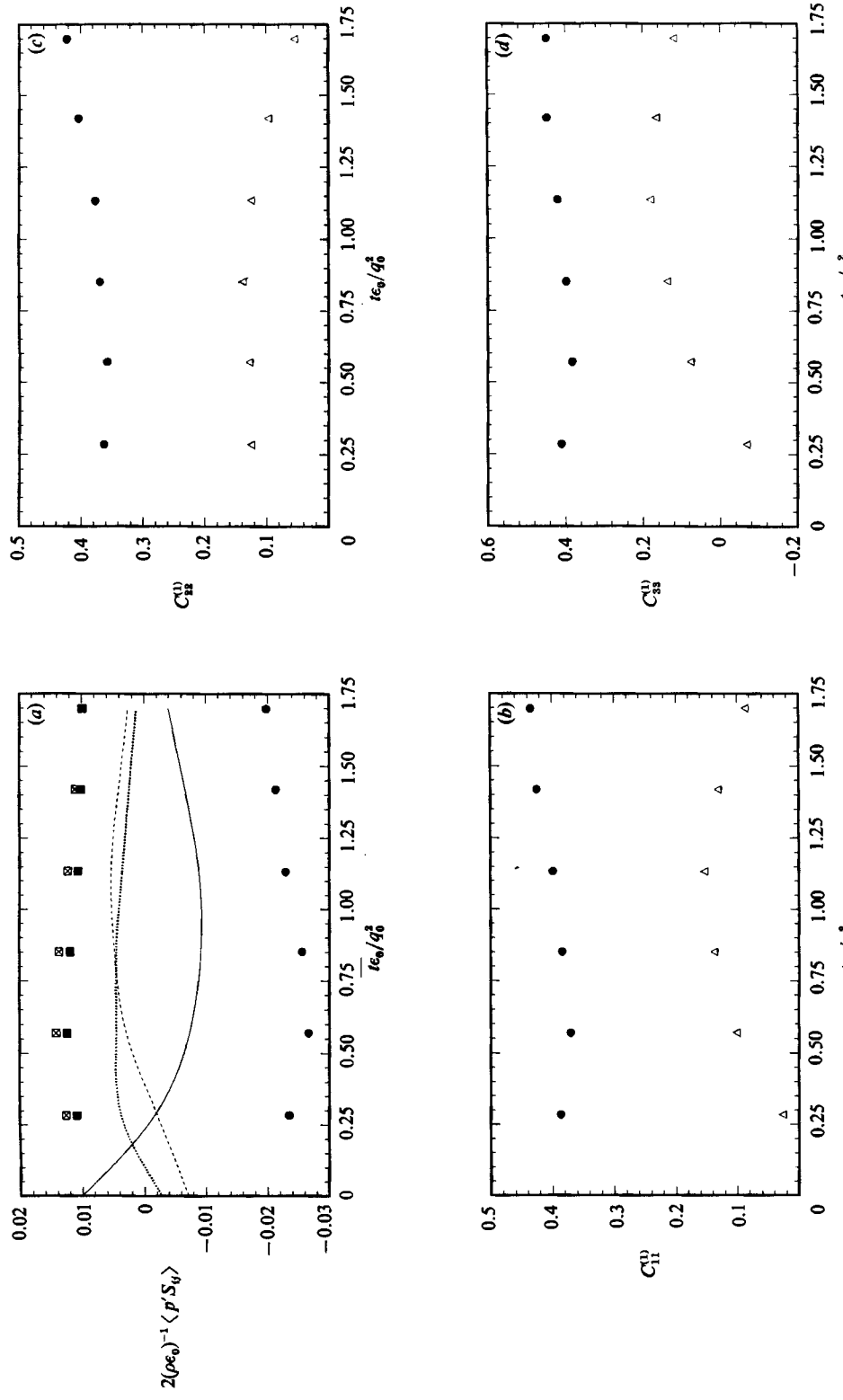

FIGURE 10. $C_{\alpha\alpha}$ and $\phi^5_{\alpha\alpha}/\epsilon_0$ versus t for an axisymmetric-expansion simulation, including both theory and simulation: (*a*), (*b*), (*c*), (*d*) are for $\phi^5_{\alpha\alpha}/\epsilon_0$, C_{11}, C_{22}, C_{33}, respectively. Symbols as in figure 5.

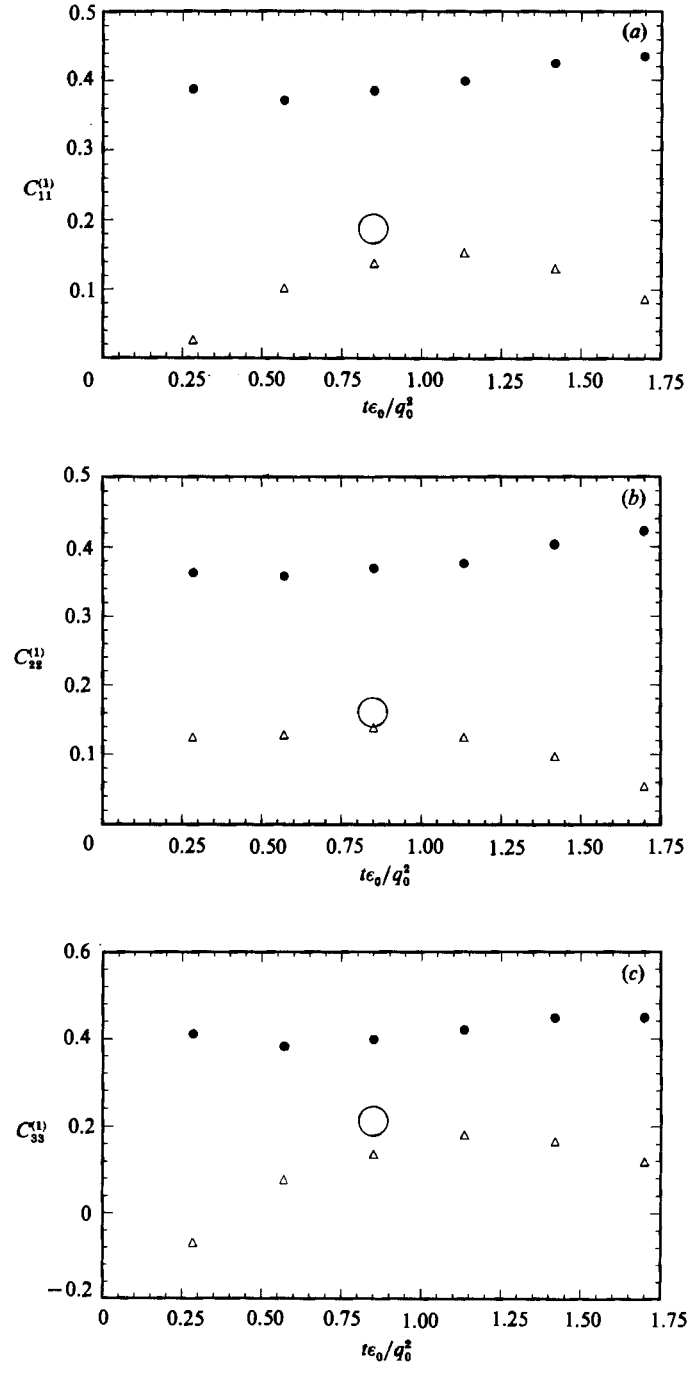

FIGURE 11. Corrected $C_{\alpha\alpha}$ for the axisymmetric expansion: ○, corrected theory at $t\epsilon_0/q_0^2 = 0.85$; ●, uncorrected theory; △, simulation. (*a*) $\alpha = 1$, (*b*) $\alpha = 2$, (*c*) $\alpha = 3$.

does not pass through zero and become negative because, for this contraction, b_{11} is never close to zero.

Whether the discrepancy is explained by non-stationarity can be determined only at the point $t\epsilon_0/q_0^2 = 0.62$ since only there are the spectra $E_{\alpha\alpha}$ available to us. At this point, the value of $C_{\alpha\alpha}$ is calculated by (6) and plotted in figure 9. It is seen that the discrepancy vanishes for C_{11}, C_{22}, and C_{33}. We have more confidence in these corrected values than for the corrected homogeneous shear values because $E_{11}/E_{22} \approx R_{11}/R_{22}$ and $E_{11}/E_{33} \approx R_{11}/R_{33}$ in most of the spectrum (see figure 5.24 of Lee & Reynolds 1985) suggesting that our approximation $\partial \ln E_{\alpha\alpha}/\partial t = \partial \ln R_{\alpha\alpha}/\partial t$ is better here.

2.4. *Axisymmetric expansion*

For an axisymmetric expansion, (simulation EXO, Lee & Reynolds 1985) the values of $C_{\alpha\alpha}$ are shown in figure 10. Upon comparison, these $C_{\alpha\alpha}$ are similar to the axisymmetric-contraction case in figure 8 – very small values with a small absolute (though large relative) difference between theory and simulation.

The discrepancy can be readily investigated for the point $t\epsilon_0/q_0^2 = 0.85$ since there the required spectra are available to us (figure 5.26 of Lee & Reynolds 1985). The corrected $C_{\alpha\alpha}$ calculated from (6) is given in figure 11. As found for the axisymmetric contraction, the discrepancy is practically removed when non-stationary is accounted for, although there is uncertainty since $\partial E_{\alpha\alpha}/\partial t$ is not known accurately.

3. Summary and discussion

3.1. *Summary*

(*a*) Both theory and simulation show that $C_{\alpha\alpha}$ varies substantially with direction and can be negative. What was anticipated is the large extent to which $C_{\alpha\alpha}$ varies with direction. Even larger variations of $C_{\alpha\alpha}$ are to be expected when the Reynolds number is allowed to increase above simulation values.

(*b*) In every case the theoretical $\phi^s_{\alpha\alpha}/\epsilon$ differed from simulations by less than 0.025.

For $C_{\alpha\alpha}$, the relative error was large for all the straining flows but the absolute error was amost always small – less than 0.3 (aside from the exception cases where $b_{\alpha\alpha}$ was extremely small ($b_{\alpha\alpha} \leqslant 0.01$) and which is discussed separately in item (*c*)). It was argued that the absolute error is more meaningful (than the relative error) since the magnitudes of $C_{\alpha\alpha}$ are small – much less than unity.

(*c*) The large discrepancies in $C_{\alpha\alpha}$ found when $b_{\alpha\alpha}$ is near zero is explainable by the fact that one is dividing by practically zero to obtain $C_{\alpha\alpha}$, i.e. since $C_{\alpha\alpha} = -\phi^s_{\alpha\alpha}/(\epsilon b_{\alpha\alpha})$ and $b_{\alpha\alpha} \approx 0$, a slight error in $b_{\alpha\alpha}$ will cause a large error in $C_{\alpha\alpha}$. Correspondingly, $C_{\alpha\alpha}$ is not a significant quantity when $|b_{\alpha\alpha}|$ is that small since, in that case $\phi^s_{\alpha\alpha}/\epsilon$ is so close to zero that it is insensitive to $C_{\alpha\alpha}$.

(*d*) In every flow point examined but one (C_{22} at $St = 4$ for homogeneous shear) the discrepancy between theory and simulation of $C_{\alpha\alpha}$ was practically eliminated when non-stationarity was accounted for. However we emphasize that corrections for non-stationarity were calculated with the severe approximation given by (7) and should be viewed with caution. One could imagine error bars of 30 % for the corrected points shown in figures 4, 7, 9 and 11.

(*e*) The non-stationary corrections are approximate because they rely on $\partial \ln E_{\alpha\alpha}/\partial t \approx \partial \ln R_{\alpha\alpha}/\partial t$. This approximation is best for the axisymmetric contraction point $t\epsilon_0/q_0^2 = 0.62$ in figure 9 and the axisymmetric expansion point $t\epsilon_0/q_0^2 = 0.85$ in figure 11 where the spectra are fairly narrowly peaked with $E_{\alpha\alpha} \propto R_{\alpha\alpha}$ near the peak.

For these two points the discrepancies are eliminated more completely than at any other points.

3.2. *Discussion*

3.2.1. *Perspective of two-point closure theory*

With an important reservation, the near agreement of prediction with simulation when non-stationarity is accounted for would lead us to conclude that two-point closures can be accurate for anisotropic flows – even when the anisotropy is very large. The reservation is that approximation (7) was used to estimate a_{rj} in (6) to calculate the non-stationary case. This approximation is crude, but may be adequate for use in (6) since there it need only be valid near the peak of $E_{\alpha\alpha}(k)$. However, the uncertainty cannot be removed until simulation values of $\partial E_{\alpha\alpha}(k)/\partial t$ become accessible for use in (6). With this reservation in mind, the comparisons for the non-stationary correction tend to confirm discard of two-time forth-order cumulants for large as well as weak anisotropy – in so far as the pressure–strain rate is concerned.

3.2.2. *Perspective of single-point modelling*

The comparisons do not provide a complete test of the theory for its application to single-point modelling because the spectra $E_{\alpha\alpha}$ were provided by the simulations. What remains, for practical applications, is to substitute an appropriate model spectrum in (2) or (4). For the sake of completeness, we note that this substitution was previously made for the following (model) spectrum: $E^{\mathrm{s}}_{\alpha\alpha} = \beta\epsilon_{\alpha\alpha}k^{-\frac{5}{3}}$ when $k_0 \leqslant k \leqslant k_\nu$ and $E^{\mathrm{s}}_{\alpha\alpha} = \beta\epsilon_{\alpha\alpha}k_0^{-m-\frac{5}{3}}k^m$ when $k \leqslant k_0$, where m is a dimensionless parameter characterizing the production regions and k_0 is an integral scale of the spectrum. (This spectrum reduces (2) to a function of $\langle u_\alpha^2\rangle$ and so makes the theory applicable to single-point models. Of particular advantage for such models, we recall, was that $\phi^{\mathrm{s}}_{\alpha\alpha}$ was found to be insensitive to m – a kind of 'universal' behaviour suggesting that $\phi^{\mathrm{s}}_{\alpha\alpha}$ is independent of the production mechanism of the turbulence.) The accuracy of using this spectral model is not directly tested in §2. Nevertheless, one could infer confirmation when the Reynolds number is very large since then the model spectrum is justifiable on theoretical grounds – particularly in the inertial subrange where most of the energy is – and (6) was found to be accurate when the correct spectrum is used. Usage of the model $E_{\alpha\alpha}$ at small Reynolds number has yet to be tested.

One last matter we mention concerns the non-stationarity correction in expression (6). Although the correction removed much of the discrepancy found between simulations and the simpler expression (2), with the reservation of (7) in mind, expression (2) may be preferred over (6) for practical usage (because it is simpler) – provided the errors in predicted $\phi^{\mathrm{s}}_{\alpha\alpha}/\epsilon$ are small. These errors are shown in figures 1, 5, 8 and 10 where the discrepancy with simulational $\phi^{\mathrm{s}}_{\alpha\alpha}/\epsilon$ is seen to be less than about 0.025 in every case. In other words, the error in the uncorrected theory is less than 2.5% of the dissipation. The question is whether this accuracy is acceptable for single-point modelling. If so, (2) without a non-stationary correction is sufficient for the flows considered here.

The author is indebted to K. Shariff for making the calculations reported here and for discussions of the pressure–strain rate, and to M. J. Lee and R. S. Rogallo for invaluable assistance in the calculations. The author is also grateful for the hospitality shown him at the CTR (Center for Turbulence Research) of Stanford University and NASA, where most of the calculations were made.

Appendix A

To derive the correction given by (6) for a non-stationary velocity spectrum $S_{ij}(\boldsymbol{k};t,t_1)$ we note that this spectrum enters ϕ^s_{ij} in bispectral forms typical of cumulant neglect theories (see Appendix A of Weinstock 1981) as

$$J_{rsij} \equiv \int \mathrm{d}\boldsymbol{k}_a \int \mathrm{d}\boldsymbol{k}_b \int_0^t \mathrm{d}t_1 S_{rs}(\boldsymbol{k}_a;t,t_1) S_{ij}(\boldsymbol{k}_b;t,t_1), \quad \boldsymbol{k}_b \equiv \boldsymbol{k}-\boldsymbol{k}_a, \tag{A 1}$$

$$S_{ij}(\boldsymbol{k}_a;t,t_1) \equiv V^{-1}\langle u_i^*(\boldsymbol{k}_a,t)\, u_j(\boldsymbol{k}_a t_1\rangle,$$

where $u_i(\boldsymbol{k},t)$ is the Fourier transform of fluctuation velocity $u_i(\boldsymbol{x},t)$ along direction i, the asterisk denotes the complex conjugate, and V is the volume of the system. We note that $S_{ij}(\boldsymbol{k};t,t_1)$ is a two-time spectrum, and, for our non-stationary case, this spectrum is not necessarily symmetric in directional components ij since $\langle u_i^2(t)\rangle$ may vary differently with t than does $\langle u_j^2(t_1)\rangle$. More specifically, ϕ^s_{ij} depends on two-time spectra in the form $J_{ij} \equiv J_{rrjt} - \frac{1}{3}J_{rrpp}\delta_{ij}$ (Weinstock 1981, 1982), i.e. ϕ^s_{ij} is proportional to

$$J_{ij} \equiv \int \frac{\mathrm{d}\boldsymbol{k}_a\, \mathrm{d}\boldsymbol{k}_b}{(2\pi)^6} \int_0^\infty \mathrm{d}t_1 M S_{rr}(\boldsymbol{k}_a;t,t_1)\,[S_{ij}(\boldsymbol{k}_b;t,t_1) - \tfrac{1}{3}S_{pp}(\boldsymbol{k}_b;t,t_1)\,\delta_{ij}], \tag{A 2}$$

where the indices r and p are summed on, and M is a well-defined function of $\boldsymbol{k}_a$ and $\boldsymbol{k}_b$ whose details are not needed for present purposes. This form is implicit in (2). The time integral in (A 2) was evaluated straightforwardly for the case of a stationary spectrum, i.e. for the case $\partial\langle u_i^*(\boldsymbol{k},t)\, u_j(\boldsymbol{k},t)\rangle/\partial t = 0$.

Our goal is to determine the time integral in (A 2) when the spectrum is non-stationary, varying with t as

$$\langle u_i^*(\boldsymbol{k},t)\, u_j(\boldsymbol{k},t)\rangle = \langle v_i^*(\boldsymbol{k},t)\, v_j(\boldsymbol{k},t)\rangle \exp(\omega_i t + \omega_j t) \tag{A 3}$$

where

$$\frac{\partial\langle v_i^*(\boldsymbol{k},t)\, v_j(\boldsymbol{k},t)\rangle}{\partial t} = 0, \tag{A 4}$$

and $\omega_i \equiv \omega_i(\boldsymbol{k},t)$ may vary with $\boldsymbol{k}$ and t. Hence, growth of $\langle u_i^* u_j^*\rangle$ is accounted for by ω_i and ω_j. To formulate an approximate two-time spectrum for use in (A 2), we need a model velocity field which satisfies (A 3) and (A 4). Such a field is given by

$$u_i(\boldsymbol{k},t) = v_i(\boldsymbol{k},t)\exp(\omega_i t) \quad (\text{model } u_i(\boldsymbol{k})). \tag{A 5}$$

where v_i is a stationary field. This model can be justified when ω_i is non-fluctuating and constant in time or when the time variations are sufficiently slow that $|\omega_i| \ll kq$. We consider the latter case. Substituting (A 5) in (A 2) we have

$$S_{ij}(\boldsymbol{k};t,t_1) = V^{-1}\langle v_i^*(\boldsymbol{k},t)\, v_j(\boldsymbol{k},t_1)\rangle \exp(\omega_i t + \omega_j t_1). \tag{A 6}$$

Now, since $v_i(\boldsymbol{k},t)$ is, by definition, a stationary field, in the sense that its magnitude is unvarying, we can use previous expressions for its self-correlation e.g. Kraichnan 1959; Weinstock 1976). In particular, at small $|t-t_1|$, wherein is the main contribution to (A 2), this correlation is

$$\langle v_i^*(\boldsymbol{k},t)\, v_j(\boldsymbol{k},t_1)\rangle \approx \langle v_i^*(\boldsymbol{k},t)\, v_j(\boldsymbol{k},t)\rangle \exp[-\tfrac{1}{6}k^2q^2(t-t_1)^2], \tag{A 7}$$

where the inequality $|\omega| \ll kq$ was employed in order to derive the simple exponent shown in (A 7) from the more accurate, but complicated, exponent

$$-\tfrac{1}{2}k^2 \int_{t_1}^{t} \mathrm{d}t_2 \int_{t_1}^{t} \mathrm{d}t_3 \langle \boldsymbol{u}(t_2)\, \boldsymbol{u}(t_3)\rangle;$$

i.e. the more accurate exponent was approximated by

$$\tfrac{1}{2}k^2(t-t_1)^2 \langle \boldsymbol{u}(t)\cdot\boldsymbol{u}(t)\rangle \equiv -\tfrac{1}{6}k^2q^2(t-t_1)^2,$$

valid when $|\omega|$ is small. Substitution of (A 7) in (A 6), followed by use of (A 5) for v_i and v_j, gives

$$S_{ij}(\boldsymbol{k}; t, t_1) = v^{-1} S_{ij}(\boldsymbol{k}) \exp\left[-\tfrac{1}{2}k^2q^2(t-t_1)^2 - \omega_j(t-t_1)\right], \tag{A 8}$$

where $S_{ij}(\boldsymbol{k}) \equiv S_{ij}(\boldsymbol{k}; t, t)$ (single-time spectrum).

Equation (A 8) is the same as the stationary case except for the growth (or decay) term $\omega_j(t-t_1)$.

To determine the change in ϕ^{s}_{ij}, caused by this growth term, (A 8) is substituted in (A 1) to obtain

$$J_{rsij} = \int \frac{\mathrm{d}\boldsymbol{k}_a\, \mathrm{d}\boldsymbol{k}_b}{(2\pi)^6} S_{rs}(\boldsymbol{k}_a)\, S_{ij}(\boldsymbol{k}_b) \int_0^t \mathrm{d}t_1 \exp\left[-\tfrac{1}{6}(k_a^2 + k_b^2)\, q^2(t-t_1)^2 - (\omega_j + \omega_s)\,(t_1 - t)\right]. \tag{A 9}$$

An adequate approximation for the t_1 integral when t is larger than $[\frac{1}{2}(k_a^2+k_b^2)\,q^2]^{-\frac{1}{2}}$ is given by

$$J_{rsij} = \int \frac{\mathrm{d}\boldsymbol{k}_a\, \mathrm{d}\boldsymbol{k}_b}{(2\pi)^3} \frac{\tau S_{rs}(\boldsymbol{k}_a)\, S_{ij}(\boldsymbol{k}_b)}{1 + a_{sj}}, \tag{A 10}$$

$$a_{sj} \equiv \tau(\omega_j + \omega_s), \quad \tau \equiv (3\pi/2)^{\frac{1}{2}} (k_a^2 + k_b^2)^{-\frac{1}{2}} q^{-1}. \tag{A 11}$$

Substituting (A 10) in (A 2) we have

$$J_{ij} \equiv \int \frac{\mathrm{d}\boldsymbol{k}_a\, \mathrm{d}\boldsymbol{k}_b}{(2\pi)^6} M\tau \sum_{r=1}^{3} S_{rr}(\boldsymbol{k}_b) \left[\frac{S_{ij}(\boldsymbol{k}_a)}{1 + a_{rj}} - \sum_{\alpha=1}^{3} \frac{S_{\alpha\alpha}(\boldsymbol{k}_a)\, \delta_{ij}}{3(1 + a_{r\alpha})}\right]. \tag{A 12}$$

Equation (A 11) reduces to the stationary case when $a_{rj} = a_{r\alpha} = 0$. As this expression implies, the non-stationary case is obtained from the stationary case by inserting the factors $(1 + a_{rj})$ as shown.

The last step in the derivation of ϕ^{s}_{ij} (e.g. Weinstock 1981) is to integrate (A 12) over spherical angles Ω_a and Ω_b of radii k_a and k_b, respectively. This integration was previously performed for $a_{rj} = 0$ (e.g. Weinstock 1981), and the same result is obtained for (A 12) except that the factors $1 + a_{rj}$ appear – provided that a_{rj} is independent of the directions of $\boldsymbol{k}_a$ and $\boldsymbol{k}_b$ or that $|a_{rj}| \ll 1$. We thus have for (A 12)

$$J_{ij} = \int \frac{\mathrm{d}k_a\, \mathrm{d}k_b}{\pi^4} d_{ij}\, \tau \sum_r E_{rr}(k_b) \left[\frac{E_{ij}(k_a)}{1 + a_{rj}} - \sum_\alpha \frac{E_{\alpha\alpha}(k_a)\, \delta_{ij}}{3(1 + a_{r\alpha})}\right], \tag{A 13}$$

where d_{ij} is a quantity that also appears in the stationary case. Again, it is seen that stationary case is converted to the non-stationary case by inserting $1 + a_{rj}$ and $1 + a_{r\alpha}$. Correspondingly, (2) is converted to the non-stationary case by replacing $E(\boldsymbol{k}_b)\,[E_{ij}(\boldsymbol{k}_a) - \frac{1}{3}E(\boldsymbol{k}_a)\,\delta_{ij}]$ with

$$\sum_r E_{rr}(k_b) \left[\frac{E_{ij}(\boldsymbol{k}_a)}{1 + a_{rj}} - \sum_\alpha \frac{E_{\alpha\alpha}(\boldsymbol{k}_a)\, \delta_{ij}}{3(1 + a_{r\alpha})}\right].$$

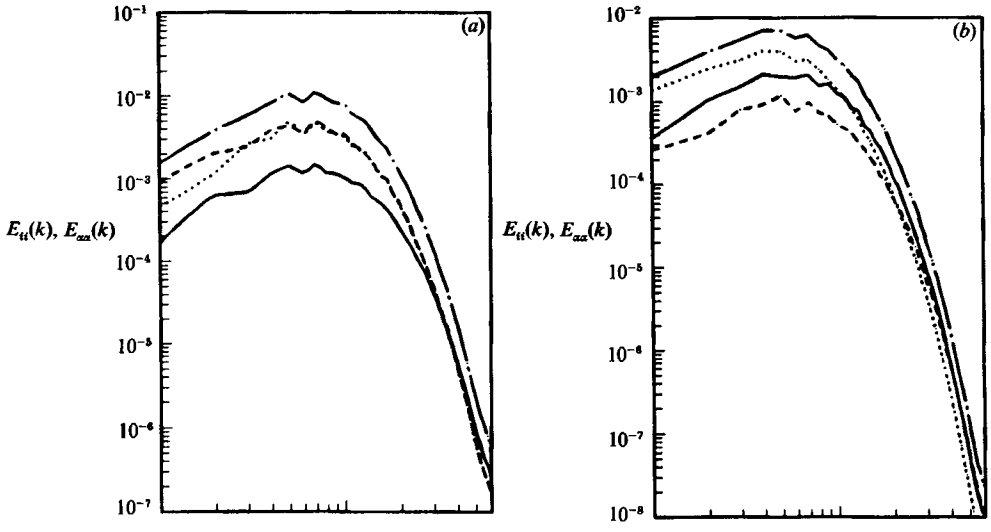

FIGURE 12. (*a*) Spectra of axisymmetric contraction at $t\epsilon_0/q_0^2 = 0.62$; (*b*) spectra of plane strain at $t\epsilon_0/q_0^2 = 0.85$.

Making this replacement in (2) yields (6), as we sought to prove. The a_{rj} in (6*b*) are defined a little differently than in (A 11), but can be seen to be the same by taking into account that ω_j in (A 3) satisfies $\omega_j = \frac{1}{2}\partial \ln E_{jj}(k_a)/\partial t$, where j is not summed on.

Appendix B

To evaluate the right-hand side of (6) we resort to the approximation

$$\frac{\partial \ln E_{\alpha\alpha}(k_a)}{\partial t} \approx \frac{\partial \ln R_{\alpha\alpha}}{\partial t}. \tag{B 1}$$

This approximation is justified if the $E_{\alpha\alpha}(k_a)$ are all proportional to each other at all k_a, i.e.

$$E_{11}(k_a) \propto E_{22}(k_a) \propto E_{33}(k_a), \tag{B 2}$$

or, at least, if the main contribution to the integrations in (6) come from a narrow region of k_a in which $E_{\alpha\alpha}(k_a)$ are proportional to $R_{\alpha\alpha}$. Where these conditions are not satisfied, corrections are made to (B 1). Study of the spectra for these simulations shows that approximation (B 2) is only fair for the homogeneous-shear and plane-strain simulations, but is very good for the axisymmetric contraction. For example, figure 12(*a*) shows that (B 2) is exceedingly well satisfied for an axisymmetric contraction at the time $t\epsilon_0/q_0^2 = 0.62$, whereas figure 12(*b*) shows that (B 2) is not as well satisfied for a plane strain.

Similarly, the homogeneous-shear spectra in figure 3 do not satisfy (B 2) for all k_a. Deviations from (B 1) are estimated by comparison with

$$\frac{\partial \ln E_{\alpha\alpha}(k_a, t)}{\partial t} \approx \frac{E_{\alpha\alpha}(k_a, t+\Delta t) - E_{\alpha\alpha}(k_a, t)}{\Delta t},$$

where Δt is the time interval between successive printouts of $E_{\alpha\alpha}$. The value of Δt is $0.35 q_0^2/\epsilon_0$ for plane strain, which is too course for other than an estimate.

Two other approximations were also used to calculate (6). The first was to replace

$$\sum_r E_{rr}\left[(1+a_{rj})^{-1}E_{ij}-\sum_\alpha \tfrac{1}{3}(1+a_{r\alpha})^{-1}E_{\alpha\alpha}\delta_{ij}\right]$$

by

$$E[(1+a_{qj})^{-1}E_{ij}-\tfrac{1}{3}(1+a_{q\alpha})^{-1}E_{\alpha\alpha}\delta_{ij}],$$

where

$$a_{qj}\equiv(3\pi/8)^{\frac{1}{2}}(k_a^2+k_b^2)^{-\frac{1}{2}}q^{-1}[\partial\ln E/\partial t+\partial\ln E_{jj}/\partial t],$$

which replacement is justified when $|a_{rj}|\ll 1$. The other approximation was to take advantage of the fact that the main contribution to the integrations in (6) and (2) is from $k_b\approx k_a$, so that the ratios of these two equations is, with (4),

$$\frac{C_{ij}}{C_{ij}^0}\approx\frac{\int_0^\infty \mathrm{d}k_a\,k_a E(k_a)[(1+a_{qj})^{-1}E_{ij}(k_a)-\sum_\alpha \tfrac{1}{3}(1+a_{q\alpha})^{-1}E_{\alpha\alpha}(k_a)\delta_{ij}]}{\int_0^\infty \mathrm{d}k_a\,k_a E(k_a)[E_{ij}(k_a)-\sum_\alpha \tfrac{1}{3}E_{\alpha\alpha}(k_a)\delta_{ij}]},\qquad\text{(B 3)}$$

where C_{ij}^0 denotes the uncorrected stationary value given by (4) and C_{ij} denotes the value corrected for non-stationarity obtained from (6). If the error made in replacing k_b by k_a in (2) and (6) is small, then it is even smaller in the ratio (B 3) since a first-order error in (2) and (6) is second order in their ratio, e.g. a 30% error in (2) and (6) is only a 10% error in (B 3). In view of the uncertainty in a_{qj} to begin with, approximation (B 3) seems justifiable. We do not expect the overall accuracy of the ratio C_{ij}/C_{ij}^0 to exceed 70 or 80%.

REFERENCES

Cambon, C., Jaendel, D. & Mathieu, J. 1981 *J. Fluid Mech.* **104**, 247–262.

Kraichnan, R. 1959 *J. Fluid Mech.* **5**, 497–543.

Launder, B. E., Reece, G. J. & Rodi, W. 1975 *J. Fluid Mech.* **68**, 537–566.

Lee, M. J. & Reynolds, W. C. 1985 *Stanford University Dept. Mech. Engng Rep.* TF-24.

Lumley, J. L. 1978 *Adv. Appl. Mech.* **18**, 123–176.

Orszag, S. A. 1970 *J. Fluid Mech.* **41**, 363–386.

Reynolds, W. C. 1976 *Ann. Rev. Phys.* **8**, 183–208.

Rogers, M. M., Moin, P. & Reynolds, W. C. 1986 *Stanford University Dept. Mech. Engng Rep.* TF-25.

Rotta, W. 1951 *Z. Phys.* **129**, 547–572.

Weinstock, J. 1976 *Phys. Fluids* **19**, 1702–1711.

Weinstock, J. 1981 *J. Fluid Mech.* **105**, 369–395.

Weinstock, J. 1982 *J. Fluid Mech.* **11**, 1–29.

Weinstock, J. & Burk, S. 1985 *J. Fluid Mech.* **154**, 429–443.